J. At. Mol. Sci.
doi: 10.4208/jams.032510.042010a

Vol. **1**, No. 3, pp. 201-214
August 2010

Theoretical Raman and IR spectra of tegafur and comparison of molecular electrostatic potential surfaces, polarizability and hyerpolarizability of tegafur with 5-fluoro-uracil by density functional theory

Onkar Prasad*, Leena Sinha, and Naveen Kumar

Department of Physics, University of Lucknow, Lucknow, Pin Code - 226007, India

Received 25 March 2010; Accepted (in revised version) 20 April 2010
Published Online 28 June 2010

Abstract. The 5-fluoro-1-(tetrahydrofuran-2-yl) pyrimidine-2,4 (1H,3H)-dione, also known as tegafur, is an important component of Tegafur-uracil (UFUR), a chemotherapy drug used in the treatment of cancer. The equilibrium geometries of "Tegafur" and 5-fluoro-uracil (5-FU) have been determined and analyzed at DFT level employing the basis set 6-311+G(d, p). The molecular electrostatic potential surface which displays the activity centres of a molecule, has been used along with frontier orbital energy gap, electric moments, first static hyperpolarizability, to interpret the better selectivity of prodrug tegafur over the drug 5-FU. The harmonic frequencies of prodrug tegafur have also been calculated to understand its complete vibrational dynamics. In general, a good agreement between experimental and calculated normal modes of vibrations has been observed.

PACS: 31.15.E-, 31.15.ap, 33.20.Tp

Key words: prodrug, polarizability, hyperpolarizability, frontier orbital energy gap, molecular electrostatic potential surface.

1 Introduction

The use of a prodrug strategy increases the selectivity and thus results in improved bioavailability of the drug for its intended target. In case of chemotherapy treatments, the reduction of adverse effects is always of paramount importance. The prodrug which is used to target the cancer cell has a low cytotoxicity, prior to its activation into cytotoxic form in the cell and hence there is a markedly lower chance of it "attacking" the healthy

*Corresponding author. *Email address:* prasad_onkar@lkouniv.ac.in (O. Prasad)

non-cancerous cells and thus reducing the side-effects associated with the chemotherapeutic agents. Tegafur, a prodrug and chemically known as 5-fluoro-1-(tetrahydrofuran-2-yl)pyrimidine-2,4(1H,3H)-dione, is an important component of 'Tegafur-uracil' (UFUR), a chemotherapy drug used in the treatment of cancer, primarily bowel cancer. UFUR is a first generation Dihydro-Pyrimidine-Dehydrogenase (DPD) inhibitory Flouropyrimidine drug. UFUR is an oral agent which combines uracil, a competitive inhibitor of DPD, with the 5-FU prodrug tegafur in a 4:1 molar ratio. Excess uracil competes with 5-FU for DPD, thus inhibiting 5-FU catabolism. The tegafur is taken up by the cancer cells and breaks down into 5-FU, a substance that kills tumor cells. The uracil causes higher amounts of 5-FU to stay inside the cells and kill them [1–4].

The present communication deals with the investigation of the structural, electronic and vibrational properties of tegafur due to its biological and medical importance in field of cancer treatment. The structure and harmonic frequencies have been determined and analyzed at DFT level employing the basis set 6-311+G(d,p). The optimized geometry of tegafur and 5-FU and their molecular properties such as equilibrium energy, frontier orbital energy gap, molecular electrostatic potential energy map, dipole moment, polarizability, first static hyperpolarizability have also been used to understand the properties and activity of the drug and prodrug. The normal mode analysis has also been carried out for better understanding of the vibrational dynamics of the molecule under investigation.

2 Computational details

Geometry optimization is one of the most important steps in the theoretical calculations. The X-ray diffraction data of the tegafur monohydrate and the drug 5-FU, obtained from Cambridge Crystallographic Data Center (CCDC) were used to generate the initial coordinates of the prodrug tegafur and drug 5-FU to optimize the structures. The Becke's three parameter hybrid exchange functionals [5] with Lee-Yang-Parr correlation functionals (B3LYP) [6,7] of the density functional theory [8] and 6-311+G(d, p) basis set were chosen. All the calculations were performed using the Gaussian 03 program [9]. The

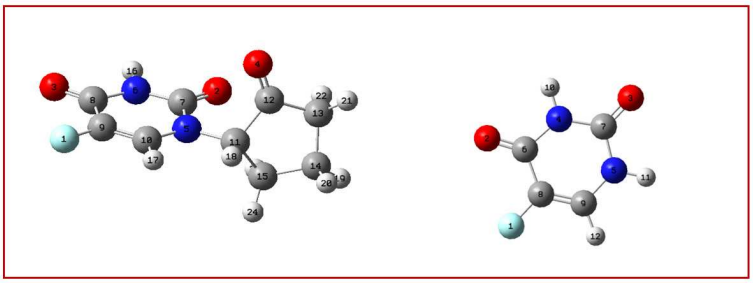

Figure 1: Optimized structure of Tegafur and 5-fluoro-uracil at B3LYP/6-311+G (d,p).

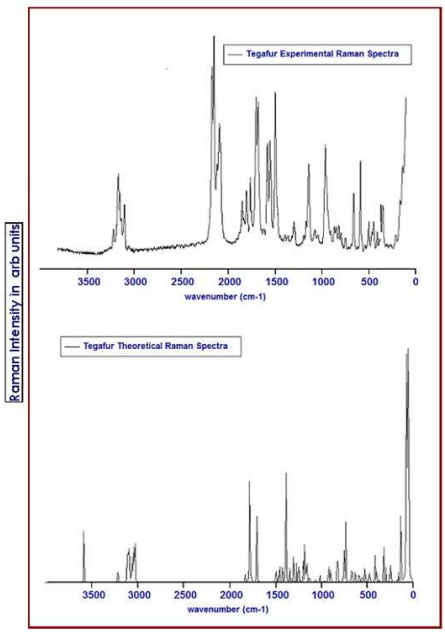

Figure 2: Experimental and theoretical Raman spectra of Tegafur.

model molecular structure of prodrug tegafur and drug 5-FU are given in the Fig.1. Positive values of all the calculated vibrational wave numbers confirmed the geometry to be located on true local minima on the potential energy surface. As the DFT hybrid B3LYP functional tends to overestimate the fundamental normal modes of vibration, a scaling factor of 0.9679 has been applied and a good agreement of calculated modes with experimental ones has been obtained [10, 11]. The vibrational frequency assignments have been carried out by combining the results of the Gaussview 3.07 program [12], symmetry considerations and the VEDA 4 program [13].

The Raman intensities were calculated from the Raman activities (Si) obtained with the Gaussian 03 program, using the following relationship derived from the intensity theory of Raman scattering [14, 15]

$$I_i = \frac{f(v_0 - v_i)^4 S_i}{v_i\{1 - \exp(-hc\, v_i/kT)\}}, \tag{1}$$

where v_0 being the exciting wave number in cm^{-1}, v_i the vibrational wave number of ith normal mode, h, c and k universal constants and f is a suitably chosen common normalization factor for all peak intensities. Raman spectra has been calculated according to the spectral database for organic compounds (SDBS) literature, using 4880 Å as exciting wavelength of laser source with 200 mW power [16]. The calculated Raman and IR spectra have been plotted using the pure Lorentzian band shape with a band width of FWHM of 3 cm^{-1} and are shown in Fig. 2 and Fig. 3, respectively.

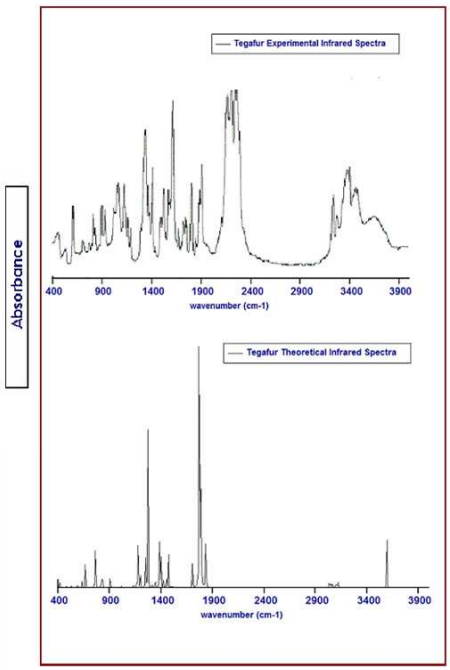

Figure 3: Experimental and theoretical IR spectra of Tegafur.

The density functional theory has also been used to calculate the dipole moment , mean polarizability $<\alpha>$ and the total first static hyperpolarizability β [17,18] are given as for both the molecules in terms of x, y, z components and are given by following equations

$$\mu = (\mu_x^2+\mu_y^2+\mu_z^2)^{1/2} \tag{2}$$

$$<\alpha> = \frac{1}{3}\left(\alpha_{xx}+\alpha_{yy}+\alpha_{zz}\right), \tag{3}$$

$$\begin{aligned}\beta_{TOTAL} &= \left(\beta_x^2+\beta_y^2+\beta_z^2\right)^{1/2} \\ &= \Big((\beta_{xxx}+\beta_{xyy}+\beta_{xzz})^2+(\beta_{yyy}+\beta_{yxx}+\beta_{yzz})^2 \\ &\quad +(\beta_{zzz}+\beta_{zxx}+\beta_{zyy})^2\Big)^{1/2}.\end{aligned} \tag{4}$$

The β components of Gaussian output are reported in atomic units and therefore the calculated values are converted into e.s.u. units (1 a.u.= 8.3693×10^{-33} e.s.u.).

3 Results and discussion

3.1 Geometric structure

The electronic structure of prodrug tegafur and the drug 5-FU have been investigated, in order to assess the effect of introduction of five-membered ring having an electron withdrawing carbonyl group to the drug 5-FU for better selectivity of target cancer cells. The optimized molecular structures with the numbering scheme of the atoms are shown in Fig. 1. The ground state optimized parameters are reported in Table 1. The five-membered ring in case of tegafur adopts an envelope conformation, with the C(14) atom, acting as the flap atom, deviating from the plane through the remaining four carbon atoms. The C-C and C-H bond lengths of five-membered rings lie in the range 1.518 Å $\sim$ 1.556 Å and 1.091 Å $\sim$ 1.096 Å respectively. The endocyclic angles of five-membered ring lie between 103.50 to 108.00 whereas there is a sharp rise in the endohedral angle values (129.1°) at N(6) atom and sharp fall in the angle values (111.3°) at C(8) atom in the six-membered hetrocyclic ring. The C(7)=O(2) / C(8)=O(3) / C(12)=O(4) bond lengths are equal to 1.217/ 1.211/ 1.202 Å and are found to be close to the standard C=O bond length (1.220 Å). These calculated bond length, bond angles are in full agreement with those reported in [19, 20]. The skeleton of tegafur molecule is non - planar while the 5-FU skeleton is planar. The optimized parameters agree well with the work reported by Teobald *et al.* [21]. The angle between the hetrocyclic six-membered ring plane and five-membered ring plane represented by ζ(N(5)-C(11)-C(15)-C(12)) is calculated at 126.1°. It is seen that most of the bond distances are similar in tegafur and 5-FU molecules, although there are differences in molecular formula. In the six-membered ring all the C-C and C-N bond distances are in the range 1.344 $\sim$ 1.457 Å and 1.382 $\sim$ 1.463 Å. According to our calculations all the carbonyl oxygen atoms carry net negative charges. The significance of this is further discussed in terms of its activity in the next section.

Table 1: Parameters corresponding to optimized geometry at DFT/ B3LYP level of theory for Tegafur and 5-FU

Parameters	Tegafur	5-FU
Ground state energy (in Hartree)	-783.639204	-514.200506
Frontier orbital energy gap (in Hartree)	0.18585	0.19593
Dipole moment (in Debye)	6.43	4.21

3.2 Electronic properties

The frontier orbitals, HOMO and LUMO determine the way a molecule interacts with other species. The frontier orbital gap helps characterize the chemical reactivity and kinetic stability of the molecule. A molecule with a small frontier orbital gap is more polarizable and is generally associated with a high chemical reactivity, low kinetic stability

and is also termed as soft molecule [22]. The frontier orbital gap in case of prodrug tegafur is found to be 0.27429 eV lower than the 5-FU molecule. The HOMO is the orbital that primarily acts as an electron donor and the LUMO is the orbital that largely acts as the electron acceptor. The 3D plots of the frontier orbitals HOMO and LUMO, electron density (ED) and the molecular electrostatic potential map (MESP) for both the molecules are shown in Fig. 4 and Fig. 5. It can be seen from the figures that, the HOMO is almost distributed uniformly in case of prodrug except the nitrogen atom between the two carbonyl groups but in case of 5-FU the HOMO is spread over the entire molecule. Homo's of both the molecules show considerable sigma bond character. The LUMO in case of tegafur is found to be shifted mainly towards hetrocyclic ring and the carbonyl group of five-membered ring and shows more antibonding character as compared to LUMO of 5-FU in which the spread of LUMO is over the entire molecule. The nodes in HOMO's and LUMO's are placed almost symmetrically. The ED plots for both molecules show a uniform distribution. The molecular electrostatic potential surface MESP which is a plot of electrostatic potential mapped onto the iso-electron density surface, simultaneously displays molecular shape, size and electrostatic potential values and has been plotted for both the molecules. Molecular electrostatic potential (MESP) mapping is very useful in the investigation of the molecular structure with its physiochemical property relationships [22–27]. The MESP map in case of tegafur clearly suggests that each carbonyl oxygen atom of the five and six- membered rings represent the most negative potential region (dark red) but the fluorine atom seems to exert comparatively small negative potential as compared to oxygen atoms. The hydrogen atoms attached to the six and five-membered ring bear the maximum brunt of positive charge (blue region). The MESP of tegafur shows clearly the three major electrophyllic active centres characterized by red colour, whereas the MESP of the 5-FU reveals two major electrophyllic active centres, the fluorine atom seems to exert almost neutral electric potential. The values of the extreme potentials on the colour scale for plotting MESP maps of both molecules have been taken same for the sake of comparison and drawing the conclusions. The predominance of green region in the MESP surfaces corresponds to a potential halfway between the two extremes red and dark blue colour. From a closer inspection of various plots given in Fig. 4 and Fig. 5 and the electronic properties listed in Table 1, one can easily conclude how the substitution of the hydrogen atom by the five-membered ring containing an electron withdrawing carbonyl group modifies the properties of the drug 5-FU.

3.3 Electric moments

The dipole moment in a molecule is an important property that is mainly used to study the intermolecular interactions involving the non bonded type dipole-dipole interactions, because higher the dipole moment, stronger will be the intermolecular interactions. The calculated value of dipole moment in case of tegafur is found to be quite higher than the drug 5-FU molecule and is attributed due to the presence of an extra highly electron withdrawing carbonyl group. The calculated dipole moment for both the molecules are

Table 2: Polarizability data/ a.u. for Tegafur at DFT/ B3LYP level of theory

Polarizability	Tegafur
α_{XX}	173.315
α_{XY}	-2.494
α_{YY}	111.365
α_{XZ}	-4.149
α_{YZ}	0.399
α_{ZZ}	92.930
$<\alpha>$	125.870

Table 3: All β components and β_{Total} for Tegafur calculated at DFT/ B3LYP level of theory

Polarizability	Tegafur
β_{XXX}	-54.9411
β_{XXY}	-57.5539
β_{XYY}	-13.4605
β_{YYY}	95.0387
β_{XXZ}	31.8370
β_{XYZ}	9.2943
β_{YYZ}	-22.0880
β_{XZZ}	57.6657
β_{YZZ}	-21.7419
β_{ZZZ}	-37.3655
β_{Total}(e.s.u.)	0.2808×10^{-30}

also given in Table 1. The lower frontier orbital energy gap and very high dipole moment for the tegafur are manifested in its high reactivity and consequently higher selectivity for the target carcinogenic / tumor cells as compared to 5-FU (refer to Table 1).

According to the present calculations, the mean polarizability of tegafur (125.870/ a.u., refer to Table 2) is found significantly higher than 5-FU (66.751/ a.u. calculated at the same level of theory as well as same basis set). This is related very well to the smaller frontier orbital gaps of tegafur as compared to 5-FU [22]. The different components of polarizability are reported in the Table 2. The first static hyperpolarizability β calculated value is found to be appreciably lowered in case of tegafur (0.2808 x 10^{-30} e.s.u., refer to Table 3) as compared to 5-FU (0.6218 x 10^{-30} e.s.u. calculated at B3LYP/ 6-311+G(d,p)). Table 3 presents the different components of static hyperpolarizability. In addition, β values do not seem to follow the same trend as α does, with the frontier orbital energy gaps. This behavior could be explained by a poor communication between the two frontier orbitals of tegafur. Although the HOMO is almost distributed uniformly in case of tegafur

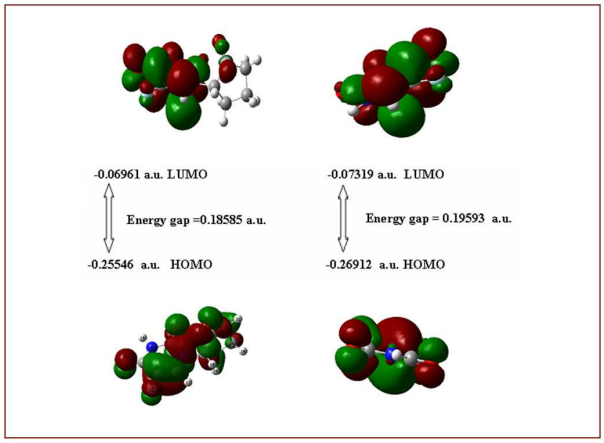

Figure 4: Plots of Homo, Lumo and the energy gaps in Tegafur and 5-FU.

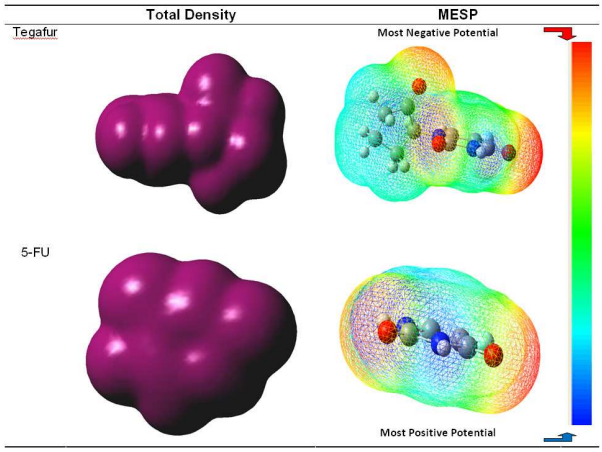

Figure 5: Total Density and MESP of Tegafur and 5-FU.

but the LUMO is found to be shrunk and shifted mainly towards hetrocyclic ring and the carbonyl group of five-membered ring and shows more antibonding character than the LUMO of 5-FU. It may thus be concluded that the higher "selectivity" of the prodrug tegafur as compared to the drug 5-FU may be attributed due to the higher dipole moment and lower values of frontier energy band gap coupled with the lower first static hyperpolarizability.

3.4 Vibrational spectral analysis

As the molecule has no symmetry, all the fundamental modes are Raman and IR active. The 66 fundamental modes of vibrations of tegafur are distributed among the functional and the finger print region. The experimental and computed vibrational wave num-

bers, their IR and Raman intensities and the detailed description of each normal mode of vibration of the prodrug tegafur, carried out in terms of their contribution to the total potential energy are given in Table 4. The calculated Raman and IR spectra of prodrug

Table 4: Theoretical and experimental a wave numbers (in cm^{-1}) of Tegafur

Exp[a] IR Wave no. in cm^{-1}	Exp[a] Raman Wave no. in cm^{-1}	Calc. (Unscaled Wave no. in cm^{-1})	Calc. (Scaled Wave no. in cm^{-1})	Calc. IR Intensity	Calc. Raman Intensity	Assignment of dominant modes in order of decreasing potential energy distribution (PED)
3426	-	3592	3477	79.83	17.38	υ(N-H)(100)
3076	3100	3219	3115	3.09	19.49	υ(C-H)R(99)
3033	-	3117	3017	14.20	12.97	υas methylene (C-H)(82)
3033	3004	3107	3007	9.87	32.29	υas methylene (C-H)(90)
-	2976	3097	2998	18.59	45.83	υas methylene (C-H)(80)
-	-	3065	2967	20.65	30.88	υs methylene (C-H)(96)
-	-	3050	2952	7.84	16.11	υ(C-H)pr(98)
-	-	3044	2946	10.24	19.02	υs methylene (C-H)(91)
2911	-	3033	2936	24.97	45.77	υs methylene (C-H)(84)
1721	-	1830	1771	208.63	7.65	$\upsilon(C_{12}$=O)pr(90)
1693	1723	1782	1725	461.25	81.78	$\upsilon(C_8$=O)R(72)
1668	1707	1766	1709	871.67	3.93	$\upsilon(C_7$=O)R(66)
1658	1661	1701	1647	76.08	42.39	$\upsilon(C_9$-$C_{10})(66)+\beta(H_{17}$-C_{10}-$C_9)(11)$
1471	1473	1511	1462	8.71	2.05	sc CH_2(93)
1466	1469	1493	1445	7.82	9.82	sc CH_2(87)
1400	1438	1467	1420	42.97	1.93	$\upsilon(N_5$-$C_)10)(23)+\beta(N_5$-C_{10}-$C_9)(13)$ $+\upsilon(N_6$-$C_8)(11)+\beta(N_5$-C_{11}-$H_{18})(10)$
1400	1403	1450	1403	20.85	7.15	sc (CH_2)(88)
1362	1367	1419	1373	8.94	3.78	$\beta(H_{16}$-N_6-$C_7)(52)+\upsilon$(C=O)R(20) $+\beta(H_{17}$-C_{10}-$N_5)(11)$
1356	1340	1393	1349	71.90	4.40	$\beta(H_{18}$-C_{11}-$N_5)(35)$ $+\beta(H_{16}$-N_6-$C_7)(13)$
1339	-	1380	1336	123.74	60.20	$\beta(H_{17}$-C_{10}-$C_9)(21)+\upsilon(C_9$-$C_{10})(14)$ $+\upsilon(N_5$-$C_{10})(13)+\upsilon(N_6$-$C_7)(12)$
-	-	1343	1300	10.26	1.21	methylene(C_{14})wag(62) +methylene(C_{15})twisting(13)
-	-	1337	1294	14.48	7.82	methylene(C_{15})wag(56) +methylene(C_{14})twisting(16)
1264	1261	1307	1266	4.21	1.73	methylene(C_{13})wag(56) +methylene(C_{14}), (C_{15})twisting(16)
1264	-	1299	1257	1.95	8.16	Methylene twisting(60)
1231	-	1267	1225	199.09	4.95	$\beta(H_{17}$-C_{10}-$N_5)(23)$ +methylene(C_{13})twisting(15) $+\upsilon(N_5$-$C_{10})(10)$
1187	-	1244	1204	85.73	9.03	Ring deformation
1179	1199	1228	1189	4.29	1.65	Methylene twisting(40) $+(C_{11}$-$H_{18})$wag(35)
-	-	1193	1155	22.23	8.09	methylene(C_{13})wag(10) $+\beta(H_{17}$-C_{10}-$C_9)(10)$

(continued)

Exp[a] IR Wave no. in cm^{-1}	Exp[a] Raman Wave no. in cm^{-1}	Calc. (Unscaled Wave no. in cm^{-1})	Calc. (Scaled Wave no. in cm^{-1})	Calc. IR Intensity	Calc. Raman Intensity	Assignment of dominant modes in order of decreasing potential energy distribution (PED)
1115	-	1168	1131	134.60	4.73	$\beta(H_{23}\text{-}C_{15}\text{-}C_{11})(21)$ +$\beta(H_{22}\text{-}C_{13}\text{-}C_{14})(18)$ $\beta(H_{16}\text{-}N_6\text{-}C_7)(17)$
1115	-	1157	1120	5.99	20.48	$\upsilon(N_6\text{-}C_7)(30)$+$\upsilon(N_5\text{-}C_{10})(16)$ +methylene twisting(14)
1065	1045	1062	1028	3.60	4.26	υ(C-C)pr(28)+$\beta(H_{18}\text{-}C_{11}\text{-}C_{12})(13)$ +methylene twisting(11)
1087	-	1126	1090	20.60	9.14	υ(C-C)pr(35)+$\beta(C_{12}\text{-}C_{13}\text{-}C_{14})(12)$
-	-	1013	980	8.56	6.79	υ(C-C)pr(54)+methylene wag(25)
941	942	965	934	2.79	1.53	υ(C-C)pr(20)+$\beta(H_{18}\text{-}C_{11}\text{-}C_{15})(17)$ +methylene twisting(10)
913	921	926	897	0.27	6.28	methylene rocking(33) +υ(C-C)pr(11)
-	-	916	886	4.13	10.06	υ(C-C)pr(59)
867	-	896	868	2.20	5.99	C-H out of plane Ring wag(79)
840	-	886	857	0.48	4.53	$\beta(H_{16}\text{-}N_6\text{-}C_7)(20)$ +$\beta(H_{17}\text{-}C_{10}\text{-}C_9)(13)$ +methylene(C_{13}) rocking(13) +methylene(C_{14}) twisting(11)
-	-	827	800	11.31	6.48	methylene rocking(69)
773	782	815	789	50.93	25.00	$\beta(C_{10}\text{-}N_5\text{-}C_7)(27)$+$\beta(C_9\text{-}C_{10}\text{-}N_5)(16)$ +υ(F-C)(11)
749	-	760	736	5.94	0.73	β_{out}(O-C-N)(78)
-	-	754	730	52.72	2.02	β_{out}(O-C-N)(77)+(N-H)wag(10)
-	-	746	722	5.53	7.78	Ring Breathing mode(51)
687	704	728	705	1.73	30.18	methylene rocking(39) +$\beta(O_2\text{-}C_7\text{-}N_6)(18)$
-	646	668	647	9.55	12.38	β(O-C-N)(45)+β(F-C-C)(11)
-	646	658	637	42.75	2.90	(N-H)wag(90)
608	-	626	606	9.55	2.91	β(C-C-C)Pr(18)+β(O-C-C)Pr(18) +(N-H)wag(12)
-	-	582	563	20.42	12.86	β_{out}(C-C-C)Pr(17)+$\beta(C_8\text{-}N_6\text{-}C_7)(12)$ +$\beta(C_9\text{-}C_{10}\text{-}N_5)(10)$
542	-	550	532	2.49	7.84	β_{out}(C-C-C)Pr(31)+β(O-C-C)Pr(15)
482	490	518	501	10.71	19.07	β(O-C-C)Pr(32) +Pr torsional mode(12) +Ring Tors. mode(12)
430	-	469	454	8.99	16.04	Pr tors. mode(31)+β(N-C-N)(23) +$\beta(N_5\text{-}C_{10}\text{-}C_9)(10)$
-	421	418	405	2.01	1.44	Pr tors. mode(29) +Ring Tors. mode(17)
-	-	410	396	7.60	8.21	Ring Tors. mode(54)

(continued)

Exp[a] IR Wave no. in cm^{-1}	Exp[a] Raman Wave no. in cm^{-1}	Calc. (Unscaled Wave no. in cm^{-1})	Calc. (Scaled Wave no. in cm^{-1})	Calc. IR Intensity	Calc. Raman Intensity	Assignment of dominant modes in order of decreasing potential energy distribution (PED)
-	381	389	377	19.53	0.39	$\beta(O_2\text{-}C_7\text{-}N_6)(22)$+Ring Tors.(21) Tors.($O_4$-$C_{11}$-$C_{13}$-$C_{12}$)(12)
-	352	364	352	3.22	8.17	Tors.(F_1-C_8-C_{10}-C_9)(59) +Tors.(O_3-N_6-C_9-C_8)(10)
-	319	312	302	1.68	0.76	$\beta(C_{10}\text{-}C_9\text{-}F_1)(26)+\beta(C_8\text{-}N_6\text{-}C_7)(18)$ $+\beta(C_{10}\text{-}N_5\text{-}C_{11})(29)$ $+\beta(C_{10}\text{-}N_5\text{-}C_7)(12)$
-	-	287	278	7.10	4.57	Ring Tors.(24)+$\beta_{out}(C_{10}\text{-}C_9\text{-}F_1)(22)$ $+\beta(C_{15}\text{-}C_{11}\text{-}N_5)(20)$
-	-	243	236	0.17	1.90	Pr tors. mode(32)+Ring Tors.(30) $+\beta_{out}(C_{10}\text{-}C_9\text{-}F_1)(12)$
-	-	230	223	1.08	1.61	Pr tors. mode(30) $+\beta(C_{10}\text{-}N_5\text{-}C_{11})(29)$
-	-	166	160	4.74	3.08	Ring Tors.(64)
-	-	152	147	2.75	4.58	Pr tors. mode(20) +Tors.(C_{15}-C_{11}-N_5-C_7)(19) +Ring Tors(10)+$\beta(C_{10}\text{-}N_5\text{-}C_{11})(10)$
-	-	128	123	0.78	3.22	Tors.(C_{15}-C_{11}-N_5-C_7)(35) +Ring Tors.(33)+Pr tors. mode(17)
-	-	74	71	1.78	1.29	Tors.(C_{14}-C_{15}-C_{11}-N_5)(61) $+\beta(C_{11}\text{-}N_5\text{-}C_{10})(10)$
-	-	61	59	1.36	1.94	Ring Tors.(36) +Tors.(C_{15}-C_{11}-N_5-C_7)(35)
-	-	45	43	1.18	1.74	Tors.(C_{11}-C_7-C_{10}-N_5)(67) +Tors.(C_{12}-C_{11}-N_5-C_7)(11)

[a] The experimental IR and Raman data have been taken from http://riodb01.ibase.aist.go.jp/sdbs website.
Note:
υ: stretching; υ_s: symmetric stretching; υ_{as}: asymmetric stretching; β: in plane bending; β_{out}: out of plane bending; Tors: torsion; sc: scissoring; ωag: wagging; Pr: Five-membered ring; Ring: Hetroaromatic six-membered ring

tegafur agree well with the experimental spectral data taken from the Spectral Database for Organic Compounds (SDBS) [16].

3.4.1 N-H vibrations

The N-H stretching of hetrocyclic six-membered ring of tegafur is calculated at 3477 cm^{-1}. As expected, this is a pure stretching mode and is evident from P.E.D. table contributing 100% to the total P.E.D., and is assigned to IR wave number at 3426 cm^{-1}. The discrepancy in the calculated and experimental N-H stretching wave number is due to the intermolecular hydrogen bonding. The mode calculated at 637 cm^{-1} represents the pure N-H wagging mode which is assigned well with the peak at 646 cm^{-1} in Raman spectra.

3.4.2 C-C and C-H vibrations

C-C stretching are observed as mixed modes in the frequency range 1600 cm^{-1} to 980 cm^{-1} for tegafur with general appearance of C-H and C-C stretching modes and are in good agreement with experimentally observed frequencies. C-C stretches are calculated to be 1090, 980, 934 and 886 cm^{-1}. The functional group region in aromatic hetrocyclic compounds exhibits weak multiple bands in the region 3100 $\sim$ 3000 cm^{-1}. The six-membered ring stretching vibrations as well as the C-H symmetric and asymmetric stretching vibrations of methylene group in tegafur are found in the region 3125 to 2925 cm^{-1}. In the present investigation, the strengthening and contraction of C-H bond C(10)-H(17) = 108.147 pm in hetrocyclic six-membered ring may have caused the C-H stretching peak to appear at 3115 cm^{-1} having almost 100% contribution to total P.E.D. in calculation. This C-H stretching vibration is assigned to the 3076 cm^{-1} IR spectra. The calculated peaks at 3017, 3007, 2998 cm^{-1} and 2967 cm^{-1} are identified as methylene asymmetric and symmetric stretching vibrations with more than 80% contribution to the total P.E.D. are matched moderately and have been assigned at 3033 cm^{-1} in the IR and at 3004 and 2976 cm^{-1} in Raman spectra respectively.

The calculated peaks in the frequency range 1475 $\sim$ 1400 cm^{-1} of tegafur correspond methylene scissoring modes with more than 85% contribution to the total P.E.D. are assigned at 1471/ 1473 and 1466/1469 cm^{-1} in the IR/ Raman spectra. Methylene wagging calculated at 1300 cm^{-1} (62% P.E.D.), 1294 and 1266 cm^{-1} (56% P.E.D. each), show considerable mixing with methylene twisting mode, whereas dominant twisting modes are calculated at 1257 cm^{-1} and 1189 cm^{-1} with 60% and 40% contribution to P.E.D. The mode calculated at 897, 800 and 705 cm^{-1} are identified as methylene rocking with their respective 33% , 69% and 39% contribution to the total P.E.D.

3.4.3 Ring vibrations

The calculated modes at 868 cm^{-1} and 722 cm^{-1} represent the pure six-membered ring wagging and breathing modes. As expected the skeletal out of plane deformations/ the torsional modes appear dominantly below the 600 cm^{-1}. The mode calculated at 789 cm^{-1} represent mixed mode with (C-C-N) and (C-N-C) in-plane bending and F-C stretching and corresponds to Raman/IR mode at 782/773 cm^{-1}. The experimental wave number at 646 cm^{-1} in Raman spectra is assigned to the in-plane (O-C-N) and (F-C-C) bending at 647 cm^{-1}.

3.4.4 C=O vibrations

The appearance of strong bands in Raman and IR spectra around 1700 to 1880 cm^{-1} show the presence of carbonyl group and is due to the C=O stretch. The frequency of the stretch due to carbonyl group mainly depends on the bond strength which in turn depends upon inductive, conjugative, field and steric effects. The three strong bands in the IR spectra at 1721, 1693 and 1668 cm^{-1} are due to C=O stretching vibrations corresponding to the three C=O groups at C(12), C(8) and C(7) respectively in tegafur. These bands are calculated

at 1771, 1725 and 1709 cm^{-1}. The discrepancy between the calculated and the observed frequencies may be due to the intermolecular hydrogen bonding.

4 Conclusions

The equilibrium geometries of tegafur and 5-FU and harmonic frequencies of tegafur molecule under investigation have been analyzed at DFT/ 6-311+G(d,p) level. In general, a good agreement between experimental and calculated normal modes of vibrations has been was observed. The skeleton of optimized tegafur molecule is non-planar. The lower frontier orbital energy gap and the higher dipole moment values make tegafur the more reactive and more polar as compared to the drug 5-FU and results in improved target cell selectivity. The molecular electrostatic potential surface and first static hyperpolarizability have also been employed successfully to explain the higher activity of tegafur over its drug 5-FU. The present study of tegafur and the corresponding drug in general may lead to the knowledge of chemical properties which are likely to improve absorption of the drug and the major metabolic pathways in the body and allow the modification of the structure of new chemical entities (drug) for the improved bioavailability.

Acknowledgments. We would like to thank Prof. Jenny Field for providing the crystal data of Tegafur and 5-FU from Cambridge Crystallographic data centre (CCDC), U. K. and Prof. M. H. Jamroz for providing his VEDA 4 software.

References

[1] L. W. Li, D. D. Wang, D. Z. Sun, M. Liu, Y. Y. Di, and H. C. Yan, Chinese Chem. Lett. 18 (2007) 891.
[2] D. Engel, A. Nudelman, N. Tarasenko, I. Levovich, I. Makarovsky, S. Sochotnikov, I. Tarasenko, and A. Rephaeli, J. Med. Chem. 51 (2008) 314.
[3] Z. Zeng, X. L. Wang, Y. D. Zhang, X. Y. Liu, W H Zhou, and N. F. Li, Pharmaceutical Development and Technology 14 (2009) 350.
[4] Z. Laura, A Azucena, C Carmen, and G Joaquin, Therapeutic Drug Monitoring 25 (2003) 221.
[5] A. D. Becke, J. Chem. Phys. 98 (1993) 5648.
[6] C. Lee, W. Yang, and R.G. Parr, Phys. Rev. B37 (1988) 785.
[7] B. Miehlich, A. Savin, H. Stoll, and H. Preuss, Chem. Phys. Lett. 157 (1989) 200.
[8] W. Kohn and L. J. Sham, Phys. Rev. 140 (1965) A1133.
[9] M. J. Frisch, G. W. Trucks, H. B. Schlegel, *et al.*, Gaussian 03, Rev. C.01 (Gaussian, Inc., Wallingford CT, 2004).
[10] A. P. Scott and L. Random, J. Phys. Chem. 100 (1996) 16502.
[11] P. Pulay, G. Fogarasi, G. Pongor, J. E. Boggs, and A. Vargha, J. Am. Chem. Soc. 105 (1983) 7037.
[12] R. Dennington, T. Keith, J. Millam, K. Eppinnett, W. L. Hovell, and R. Gilliland, GaussView, Version 3.07 (Semichem, Inc., Shawnee Mission, KS, 2003).

[13] M. H. Jamroz, Vibrational Energy Distribution Analysis: VEDA 4 Program (Warsaw, Poland, 2004).
[14] G. Keresztury, S. Holly, J.Varga, G. Besenyei, A. Y. Wang, and J. R. Durig, Spectrochim. Acta 49 A (1993) 2007.
[15] G. Keresztury, Raman spectroscopy theory, in: Handbook of Vibrational Spectroscopy, Vol. 1, eds. J.M. Chalmers and P. R. Griffith (John Wiley & Sons, New York, 2002) pp. 1.
[16] http://riodb01.ibase.aist.go.jp/sdbs/ (National Institute of Advanced Industrial Science and Technologys, Japan)
[17] D. A. Kleinman, Phys, Rev. 126 (1962) 1977.
[18] J. Pipek and P. Z. Mezey, J. Chem. Phys. 90 (1989) 4916.
[19] M. Ladd, Introduction to Physical Chemistry, third ed. (Cambridge University Press, Cambridge, 1998).
[20] F. H. Allen, O. Kennard, and D. G. Watson, J. Chem. Soc., Perkin Trans. 2 (S1) (1987) 12.
[21] B. Blicharska and T. Kupka, J. Mol. Struct. 613 (2002) 153.
[22] I. Fleming, Frontier Orbitals and Organic Chemical Reactions (John Wiley and Sons, New York, 1976) pp. 5-27.
[23] J. S. Murray and K. Sen, Molecular Electrostatic Potentials, Concepts and Applications (Elsevier, Amsterdam, 1996).
[24] I. Alkorta and J. J. Perez, Int. J. Quant. Chem. 57 (1996) 123.
[25] E. Scrocco and J. Tomasi, Advances in Quantum Chemistry, Vol. 11 (Academic Press, New York, 1978) pp. 115.
[26] F. J. Luque, M. Orozco, P. K. Bhadane, and S. R. Gadre, J. Phys. Chem. 97 (1993) 9380.
[27] J. Sponer and P. Hobza, Int. J. Quant. Chem. 57 (1996) 959.